Figure 5. Transfection of TIG-1 cells with multiple genes using PEI max-MNPs. TIG-1 cells were simultaneously transfected with GFP, CFP, and YFP expression vector plasmids. TIG-1 cells were treated with 0.8 μg of PEI max-MNPs and 0.7 μg each of pCAG-GFP (GFP, provided by Dr. Nishino), pPhi-Yellow-N (YFP, Evrogen), and pAmCyan1-C1 (CFP, Clonetech) for 8 h on the magnetic plate in a six-well plate or a 35 mm dish. White bar indicates 200 μm.

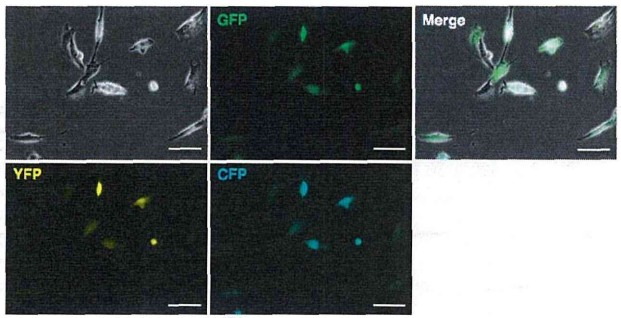

5. Conclusions

The great promise of gene therapy for treating devastating, incurable diseases has yet to be realized. Less toxic and more efficient systems will be required, and robust research efforts in this regard are currently underway. Rapid advances have been made in adapting nanoparticle technology for basic biomedical and clinical research. Nanoparticles are already being used clinically to enhance MRI imaging, and drug delivery for cancer patients. Our own research has focused on gene delivery systems for autologous cell transplantation therapy, in which the patient's own cells are transfected with the gene required to correct their condition. In particular, our laboratory and those of others have aimed to optimize magnetofection by developing better nanoparticle coating agents [38,40–51,53–55]. Nanoparticle size is another important parameter but there were few reports addressing this subject [111]. Since cells endocytose MNPs [51,100,101], MNP size has significant implications for transfection efficiency. PEI-MNPs forms magnetoplex, which increased its influence on the magnetic force. Furthermore, MNP size influences cytotoxicity [112], and more studies on this aspect of MNP technology will be crucial for enhancing transfection efficiencies.

The two research groups reported the important developments in the field of magnetofection. The first is the influence of the oscillating magnetic force on transfection [113,114]. The second is the use of MNP-heating, and -transfection [15,16]. The purpose of these studies have increased the efficiency of transfection, and/or induced a fever by oscillating MNPs for hyperthermia. The latter, a combination of MNP-heating and -transfection, was expected to research the efficacy of both hyperthermia and gene delivery. In the future, the studies of magnetofection using the oscillating MNPs could be developed as a novel methodology.

We found that PEI is an excellent cationic polymer for dispersing MNPs and that its water solubility, stability, and low toxicity contribute to enhancing transfection efficiency [95,115–119].

Derivation of iPSCs with the use of non-viral gene delivery using PEI max MNPs should provide a powerful tool for treating diseases such as Alzheimer's, Huntington's, and Parkinson's by autologous cell transplantation. Reprogramming cells requires the action of multiple transcription factors. Our studies demonstrate that MNP-mediated transfection efficiently introduces at least three genes in a single cell. This indicates the feasibility of our system for one-step reprogramming.

References

1. Chouly, C.; Pouliquen, D.; Lucet, I.; Jeune, J.J.; Jallet, P. Development of superparamagnetic nanoparticles for MRI: Effect of particle size, charge and surface nature on biodistribution. *J. Microencapsul.* **1996**, *13*, 245–255.
2. Schlorf, T.; Meincke, M.; Kossel, E.; Gluer, C.C.; Jansen, O.; Mentlein, R. Biological properties of iron oxide nanoparticles for cellular and molecular magnetic resonance imaging. *Int. J. Mol. Sci.* **2010**, *12*, 12–23.
3. Yoo, B.; Pagel, M.D. An overview of responsive MRI contrast agents for molecular imaging. *Front. Biosci.* **2008**, *13*, 1733–1752.
4. Sun, C.; Fang, C.; Stephen, Z.; Veiseh, O.; Hansen, S.; Lee, D.; Ellenbogen, R.G.; Olson, J.; Zhang, M. Tumor-targeted drug delivery and MRI contrast enhancement by chlorotoxin-conjugated iron oxide nanoparticles. *Nanomedicine (Lond. UK)* **2008**, *3*, 495–505.
5. Medarova, Z.; Rashkovetsky, L.; Pantazopoulos, P.; Moore, A. Multiparametric monitoring of tumor response to chemotherapy by noninvasive imaging. *Cancer Res.* **2009**, *69*, 1182–1189.
6. Wu, Y.L.; Ye, Q.; Sato, K.; Foley, L.M.; Hitchens, T.K.; Ho, C. Noninvasive evaluation of cardiac allograft rejection by cellular and functional cardiac magnetic resonance. *JACC Cardiovasc. Imaging* **2009**, *2*, 731–741.
7. Wu, Y.L.; Ye, Q.; Foley, L.M.; Hitchens, T.K.; Sato, K.; Williams, J.B.; Ho, C. *In situ* labeling of immune cells with iron oxide particles: An approach to detect organ rejection by cellular MRI. *Proc. Natl. Acad. Sci. USA* **2006**, *103*, 1852–1857.
8. Chen, C.L.; Zhang, H.; Ye, Q.; Hsieh, W.Y.; Hitchens, T.K.; Shen, H.H.; Liu, L.; Wu, Y.J.; Foley, L.M.; Wang, S.J.; *et al.* A New Nano-sized Iron Oxide Particle with High Sensitivity for Cellular Magnetic Resonance Imaging. *Mol. Imaging Biol.* **2010**, doi:10.1007/s11307-010-0430-x.
9. Matsumura, Y.; Maeda, H. A new concept for macromolecular therapeutics in cancer chemotherapy: Mechanism of tumoritropic accumulation of proteins and the antitumor agent smancs. *Cancer Res.* **1986**, *46*, 6387–6392.
10. Maeda, H.; Matsumura, Y. Tumoritropic and lymphotropic principles of macromolecular drugs. *Crit. Rev. Ther. Drug Carrier Syst.* **1989**, *6*, 193–210.
11. Oh, K.T.; Baik, H.J.; Lee, A.H.; Oh, Y.T.; Youn, Y.S.; Lee, E.S. The reversal of drug-resistance in tumors using a drug-carrying nanoparticular system. *Int. J. Mol. Sci.* **2009**, *10*, 3776–3792.
12. Jordan, A.; Scholz, R.; Wust, P.; Fahling, H.; Roland, F. Magnetic fluid hyperthermia (MFH): Cancer treatment with AC magnetic field induced excitation of biocompatible superparamagnetic nanoparticles. *J. Magn. Magn. Mater.* **1999**, *201*, 413–419.

13. Mornet, S.; Vasseur, S.; Grasset, F.; Veverka, P.; Goglio, G.; Demourgues, A.; Portier, J.; Pollert, E.; Duguet, E. Magnetic nanoparticle design for medical applications. *Prog. Solid State Chem.* **2006**, *34*, 237–247.
14. Kim, D.H.; Kim, K.N.; Kim, K.M.; Lee, Y.K. Targeting to carcinoma cells with chitosan- and starch-coated magnetic nanoparticles for magnetic hyperthermia. *J. Biomed. Mater. Res., Part A* **2009**, *88*, 1–11.
15. Ito, A.; Shinkai, M.; Honda, H.; Kobayashi, T. Heat-inducible TNF-alpha gene therapy combined with hyperthermia using magnetic nanoparticles as a novel tumor-targeted therapy. *Cancer Gene Ther.* **2001**, *8*, 649–654.
16. Tang, Q.S.; Zhang, D.S.; Cong, X.M.; Wan, M.L.; Jin, L.Q. Using thermal energy produced by irradiation of Mn-Zn ferrite magnetic nanoparticles (MZF-NPs) for heat-inducible gene expression. *Biomaterials* **2008**, *29*, 2673–2679.
17. Salloum, M.; Ma, R.H.; Weeks, D.; Zhu, L. Controlling nanoparticle delivery in magnetic nanoparticle hyperthermia for cancer treatment: Experimental study in agarose gel. *Int. J. Hyperthermia* **2008**, *24*, 337–345.
18. Wust, P.; Gneveckow, U.; Johannsen, M.; Bohmer, D.; Henkel, T.; Kahmann, F.; Sehouli, J.; Felix, R.; Ricke, J.; Jordan, A. Magnetic nanoparticles for interstitial thermotherapy—feasibility, tolerance and achieved temperatures. *Int. J. Hyperth.* **2006**, *22*, 673–685.
19. Ito, A.; Honda, H.; Kobayashi, T. Cancer immunotherapy based on intracellular hyperthermia using magnetite nanoparticles: A novel concept of "heat-controlled necrosis" with heat shock protein expression. *Cancer Immunol. Immunother.* **2006**, *55*, 320–328.
20. Tanaka, K.; Ito, A.; Kobayashi, T.; Kawamura, T.; Shimada, S.; Matsumoto, K.; Saida, T.; Honda, H. Intratumoral injection of immature dendritic cells enhances antitumor effect of hyperthermia using magnetic nanoparticles. *Int. J. Cancer* **2005**, *116*, 624–633.
21. Ito, A.; Tanaka, K.; Honda, H.; Abe, S.; Yamaguchi, H.; Kobayashi, T. Complete regression of mouse mammary carcinoma with a size greater than 15 mm by frequent repeated hyperthermia using magnetite nanoparticles. *J. Biosci. Bioeng.* **2003**, *96*, 364–369.
22. Muggia, F.M. Doxorubicin-polymer conjugates: Further demonstration of the concept of enhanced permeability and retention. *Clin. Cancer Res.* **1999**, *5*, 7–8.
23. Gabizon, A.; Chemla, M.; Tzemach, D.; Horowitz, A.T.; Goren, D. Liposome longevity and stability in circulation: Effects on the *in vivo* delivery to tumors and therapeutic efficacy of encapsulated anthracyclines. *J. Drug Target.* **1996**, *3*, 391–398.
24. Sakakibara, T.; Chen, F.A.; Kida, H.; Kunieda, K.; Cuenca, R.E.; Martin, F.J.; Bankert, R.B. Doxorubicin encapsulated in sterically stabilized liposomes is superior to free drug or drug-containing conventional liposomes at suppressing growth and metastases of human lung tumor xenografts. *Cancer Res.* **1996**, *56*, 3743–3746.
25. Harrington, K.J.; Mohammadtaghi, S.; Uster, P.S.; Glass, D.; Peters, A.M.; Vile, R.G.; Stewart, J.S. Effective targeting of solid tumors in patients with locally advanced cancers by radiolabeled pegylated liposomes. *Clin. Cancer Res.* **2001**, *7*, 243–254.
26. Noe, L.L.; Becker, R.V., III; Gradishar, W.J.; Gore, M.; Trotter, J.P. The cost effectiveness of tamoxifen in the prevention of breast cancer. *Am. J. Manag. Care* **1999**, *5* (Suppl. 6), S389–S406.

27. Ibrahim, N.K.; Desai, N.; Legha, S.; Soon-Shiong, P.; Theriault, R.L.; Rivera, E.; Esmaeli, B.; Ring, S.E.; Bedikian, A.; Hortobagyi, G.N.; *et al.* Phase I and pharmacokinetic study of ABI-007, a Cremophor-free, protein-stabilized, nanoparticle formulation of paclitaxel. *Clin. Cancer Res.* **2002**, *8*, 1038–1044.
28. Ibrahim, N.K.; Samuels, B.; Page, R.; Doval, D.; Patel, K.M.; Rao, S.C.; Nair, M.K.; Bhar, P.; Desai, N.; Hortobagyi, G.N. Multicenter phase II trial of ABI-007, an albumin-bound paclitaxel, in women with metastatic breast cancer. *J. Clin. Oncol.* **2005**, *23*, 6019–6026.
29. Pinder, M.C.; Ibrahim, N.K. Nanoparticle albumin-bound paclitaxel for treatment of metastatic breast cancer. *Drugs Today* **2006**, *42*, 599–604.
30. Hamaguchi, T.; Kato, K.; Yasui, H.; Morizane, C.; Ikeda, M.; Ueno, H.; Muro, K.; Yamada, Y.; Okusaka, T.; Shirao, K.; *et al.* A phase I and pharmacokinetic study of NK105, a paclitaxel-incorporating micellar nanoparticle formulation. *Br. J. Cancer* **2007**, *97*, 170–176.
31. Hamaguchi, T.; Matsumura, Y.; Suzuki, M.; Shimizu, K.; Goda, R.; Nakamura, I.; Nakatomi, I.; Yokoyama, M.; Kataoka, K.; Kakizoe, T. NK105, a paclitaxel-incorporating micellar nanoparticle formulation, can extend *in vivo* antitumour activity and reduce the neurotoxicity of paclitaxel. *Br. J. Cancer* **2005**, *92*, 1240–1246.
32. Muggia, F.M.; Hainsworth, J.D.; Jeffers, S.; Miller, P.; Groshen, S.; Tan, M.; Roman, L.; Uziely, B.; Muderspach, L.; Garcia, A.; *et al.* Phase II study of liposomal doxorubicin in refractory ovarian cancer: Antitumor activity and toxicity modification by liposomal encapsulation. *J. Clin. Oncol.* **1997**, *15*, 987–993.
33. Kikumori, T.; Kobayashi, T.; Sawaki, M.; Imai, T. Anti-cancer effect of hyperthermia on breast cancer by magnetite nanoparticle-loaded anti-HER2 immunoliposomes. *Breast Cancer Res. Treat.* **2009**, *113*, 435–441.
34. Johannsen, M.; Thiesen, B.; Wust, P.; Jordan, A. Magnetic nanoparticle hyperthermia for prostate cancer. *Int. J. Hyperth.* **2010**, *26*, 790–795.
35. Rao, W.; Deng, Z.S.; Liu, J. A review of hyperthermia combined with radiotherapy/chemotherapy on malignant tumors. *Crit. Rev. Biomed. Eng.* **2010**, *38*, 101–116.
36. Yallapu, M.M.; Othman, S.F.; Curtis, E.T.; Gupta, B.K.; Jaggi, M.; Chauhan, S.C. Multi-functional magnetic nanoparticles for magnetic resonance imaging and cancer therapy. *Biomaterials* **2011**, *32*, 1890–1905.
37. Chen, B.; Wu, W.; Wang, X. Magnetic iron oxide nanoparticles for tumor-targeted therapy. *Curr. Cancer Drug Targets* **2011**, *11*, 184–189.
38. Zhang, H.; Lee, M.Y.; Hogg, M.G.; Dordick, J.S.; Sharfstein, S.T. Gene delivery in three-dimensional cell cultures by superparamagnetic nanoparticles. *ACS Nano* **2010**, *4*, 4733–4743.
39. Pickard, M.R.; Barraud, P.; Chari, D.M. The transfection of multipotent neural precursor/stem cell transplant populations with magnetic nanoparticles. *Biomaterials* **2011**, *32*, 2274–2284.
40. Lee, J.H.; Lee, K.; Moon, S.H.; Lee, Y.; Park, T.G.; Cheon, J. All-in-one target-cell-specific magnetic nanoparticles for simultaneous molecular imaging and siRNA delivery. *Angew. Chem., Int. Ed. Engl.* **2009**, *48*, 4174–4179.

41. Kievit, F.M.; Veiseh, O.; Bhattarai, N.; Fang, C.; Gunn, J.W.; Lee, D.; Ellenbogen, R.G.; Olson, J.M.; Zhang, M. PEI-PEG-Chitosan Copolymer Coated Iron Oxide Nanoparticles for Safe Gene Delivery: Synthesis, complexation, and transfection. *Adv. Funct. Mater.* **2009**, *19*, 2244–2251.
42. Mykhaylyk, O.; Antequera, Y.S.; Vlaskou, D.; Plank, C. Generation of magnetic nonviral gene transfer agents and magnetofection *in vitro*. *Nat. Protoc.* **2007**, *2*, 2391–2411.
43. Song, H.P.; Yang, J.Y.; Lo, S.L.; Wang, Y.; Fan, W.M.; Tang, X.S.; Xue, J.M.; Wang, S. Gene transfer using self-assembled ternary complexes of cationic magnetic nanoparticles, plasmid DNA and cell-penetrating Tat peptide. *Biomaterials* **2010**, *31*, 769–778.
44. Scherer, F.; Anton, M.; Schillinger, U.; Henke, J.; Bergemann, C.; Kruger, A.; Gansbacher, B.; Plank, C. Magnetofection: Enhancing and targeting gene delivery by magnetic force *in vitro* and *in vivo*. *Gene Ther.* **2002**, *9*, 102–109.
45. Shi, Y.; Zhou, L.; Wang, R.; Pang, Y.; Xiao, W.; Li, H.; Su, Y.; Wang, X.; Zhu, B.; Zhu, X.; Yan, D.; Gu, H. *In situ* preparation of magnetic nonviral gene vectors and magnetofection *in vitro*. *Nanotechnology* **2010**, *21*, 115103.
46. Ang, D.; Nguyen, Q.V.; Kayal, S.; Preiser, P.R.; Rawat, R.S.; Ramanujan, R.V. Insights into the mechanism of magnetic particle assisted gene delivery. *Acta Biomater.* **2011**, *7*, 1319–1326.
47. Morishita, N.; Nakagami, H.; Morishita, R.; Takeda, S.; Mishima, F.; Terazono, B.; Nishijima, S.; Kaneda, Y.; Tanaka, N. Magnetic nanoparticles with surface modification enhanced gene delivery of HVJ-E vector. *Biochem. Biophys. Res. Commun.* **2005**, *334*, 1121–1126.
48. Namgung, R.; Singha, K.; Yu, M.K.; Jon, S.; Kim, Y.S.; Ahn, Y.; Park, I.K.; Kim, W.J. Hybrid superparamagnetic iron oxide nanoparticle-branched polyethylenimine magnetoplexes for gene transfection of vascular endothelial cells. *Biomaterials* **2010**, *31*, 4204–4213.
49. Yiu, H.H.; McBain, S.C.; Lethbridge, Z.A.; Lees, M.R.; Dobson, J. Preparation and characterization of polyethylenimine-coated Fe_3O_4-MCM-48 nanocomposite particles as a novel agent for magnet-assisted transfection. *J. Biomed. Mater. Res., Part A* **2010**, *92*, 386–392.
50. Namiki, Y.; Namiki, T.; Yoshida, H.; Ishii, Y.; Tsubota, A.; Koido, S.; Nariai, K.; Mitsunaga, M.; Yanagisawa, S.; Kashiwagi, H.; *et al.* A novel magnetic crystal-lipid nanostructure for magnetically guided *in vivo* gene delivery. *Nat. Nanotechnol.* **2009**, *4*, 598–606.
51. Arsianti, M.; Lim, M.; Marquis, C.P.; Amal, R. Polyethylenimine based magnetic iron-oxide vector: The effect of vector component assembly on cellular entry mechanism, intracellular localization, and cellular viability. *Biomacromolecules* **2010**, *11*, 2521–3251.
52. Kim, T.S.; Lee, S.H.; Gang, G.T.; Lee, Y.S.; Kim, S.U.; Koo, D.B.; Shin, M.Y.; Park, C.K.; Lee, D.S. Exogenous DNA uptake of boar spermatozoa by a magnetic nanoparticle vector system. *Reprod. Domest. Anim.* **2009**, *45*, e201–e206.
53. Yang, S.Y.; Sun, J.S.; Liu, C.H.; Tsuang, Y.H.; Chen, L.T.; Hong, C.Y.; Yang, H.C.; Horng, H.E. *Ex vivo* magnetofection with magnetic nanoparticles: A novel platform for nonviral tissue engineering. *Artif. Organs* **2008**, *32*, 195–204.
54. Tresilwised, N.; Pithayanukul, P.; Mykhaylyk, O.; Holm, P.S.; Holzmuller, R.; Anton, M.; Thalhammer, S.; Adiguzel, D.; Doblinger, M.; Plank, C. Boosting oncolytic adenovirus potency with magnetic nanoparticles and magnetic force. *Mol. Pharmaceutics* **2010**, *7*, 1069–1089.

55. Hashimoto, M.; Hisano, Y. Directional gene-transfer into the brain by an adenoviral vector tagged with magnetic nanoparticles. *J. Neurosci. Methods* **2011**, *194*, 316–320.
56. Mah, C.; Fraites, T.J., Jr.; Zolotukhin, I.; Song, S.; Flotte, T.R.; Dobson, J.; Batich, C.; Byrne, B.J. Improved method of recombinant AAV2 delivery for systemic targeted gene therapy. *Mol. Ther.* **2002**, *6*, 106–112.
57. Basti, H.; Ben Tahar, L.; Smiri, L.S.; Herbst, F.; Vaulay, M.J.; Chau, F.; Ammar, S.; Benderbous, S. Catechol derivatives-coated Fe_3O_4 and gamma-Fe_2O_3 nanoparticles as potential MRI contrast agents. *J. Colloid Interface Sci.* **2010**, *341*, 248–254.
58. Gamarra, L.F.; Amaro, E., Jr.; Alves, S.; Soga, D.; Pontuschka, W.M.; Mamani, J.B.; Carneiro, S.M.; Brito, G.E.; Figueiredo Neto, A.M. Characterization of the biocompatible magnetic colloid on the basis of Fe_3O_4 nanoparticles coated with dextran, used as contrast agent in magnetic resonance imaging. *J. Nanosci. Nanotechnol.* **2010**, *10*, 4145–4153.
59. Jung, C.W.; Jacobs, P. Physical and chemical properties of superparamagnetic iron oxide MR contrast agents: Ferumoxides, ferumoxtran, ferumoxsil. *Magn. Reson. Imaging* **1995**, *13*, 661–674.
60. Martina, M.S.; Fortin, J.P.; Menager, C.; Clement, O.; Barratt, G.; Grabielle-Madelmont, C.; Gazeau, F.; Cabuil, V.; Lesieur, S. Generation of superparamagnetic liposomes revealed as highly efficient MRI contrast agents for *in vivo* imaging. *J. Am. Chem. Soc.* **2005**, *127*, 10676–10685.
61. Widder, D.J.; Greif, W.L.; Widder, K.J.; Edelman, R.R.; Brady, T.J. Magnetite albumin microspheres: A new MR contrast material. *Am. J. Roentgenol.* **1987**, *148*, 399–404.
62. Sun, X.; Gutierrez, A.; Yacaman, M.J.; Dong, X.; Jin, S. Investigations on magnetic properties and structure for carbon encapsulated nanoparticles of Fe, Co, Ni. *Mater. Sci. Eng. A* **2000**, *286*, 157–160.
63. Tomitaka, A.; Kobayashi, H.; Yamada, T.; Jeun, M.; Bae, S.; Takemura, Y. Magnetization and self-heating temperature of $NiFe_2O_4$ nanoparticles measured by applying ac magnetic field. *J. Phys.: Conf. Ser.* **2010**, *200*, 122010.
64. Cho, W.S.; Duffin, R.; Poland, C.A.; Duschl, A.; Oostingh, G.J.; Macnee, W.; Bradley, M.; Megson, I.L.; Donaldson, K. Differential pro-inflammatory effects of metal oxide nanoparticles and their soluble ions *in vitro* and *in vivo*; zinc and copper nanoparticles, but not their ions, recruit eosinophils to the lungs. *Nanotoxicology* **2011**, in press.
65. George, S.; Xia, T.; Rallo, R.; Zhao, Y.; Ji, Z.; Lin, S.; Wang, X.; Zhang, H.; France, B.; Schoenfeld, D.; *et al.* Use of a high-throughput screening approach coupled with *in vivo* zebrafish embryo screening to develop hazard ranking for engineered nanomaterials. *ACS Nano* **2011**, *5*, 1805–1817.
66. Giri, J.; Pradhan, P.; Somani, V.; Chelawat, H.; Chhatre, S.; Banerjee, R.; Bahadur, D. Synthesis and characterizations of water-based ferrofluids of substituted ferrites [Fe1-xBxFe2O4, B = Mn, Co ($x = 0-1$)] for biomedical applications. *J. Magn. Magn. Mater.* **2008**, *320*, 724–730.
67. Karlsson, H.L.; Cronholm, P.; Gustafsson, J.; Moller, L. Copper oxide nanoparticles are highly toxic: A comparison between metal oxide nanoparticles and carbon nanotubes. *Chem. Res. Toxicol.* **2008**, *21*, 1726–1732.

68. McBain, S.C.; Yiu, H.H.; Dobson, J. Magnetic nanoparticles for gene and drug delivery. *Int. J. Nanomed.* **2008**, *3*, 169–180.
69. Buyukhatipoglu, K.; Clyne, A.M. Superparamagnetic iron oxide nanoparticles change endothelial cell morphology and mechanics via reactive oxygen species formation. *J. Biomed. Mater. Res., Part A* **2011**, *96*, 186–195.
70. Schroder, U.; Segren, S.; Gemmefors, C.; Hedlund, G.; Jansson, B.; Sjogren, H.O.; Borrebaeck, C.A. Magnetic carbohydrate nanoparticles for affinity cell separation. *J. Immunol. Methods* **1986**, *93*, 45–53.
71. Berry, C.C.; Wells, S.; Charles, S.; Curtis, A.S. Dextran and albumin derivatised iron oxide nanoparticles: Influence on fibroblasts *in vitro*. *Biomaterials* **2003**, *24*, 4551–7455.
72. Nitin, N.; LaConte, L.E.; Zurkiya, O.; Hu, X.; Bao, G. Functionalization and peptide-based delivery of magnetic nanoparticles as an intracellular MRI contrast agent. *J. Biol. Inorg. Chem.* **2004**, *9*, 706–712.
73. Ito, A.; Ino, K.; Kobayashi, T.; Honda, H. The effect of RGD peptide-conjugated magnetite cationic liposomes on cell growth and cell sheet harvesting. *Biomaterials* **2005**, *26*, 6185–6193.
74. de la Fuente, J.M.; Penades, S. Glyconanoparticles: Types, synthesis and applications in glycoscience, biomedicine and material science. *Biochim. Biophys. Acta* **2006**, *1760*, 636–651.
75. McDonald, M.A.; Watkin, K.L. Investigations into the physicochemical properties of dextran small particulate gadolinium oxide nanoparticles. *Acad. Radiol.* **2006**, *13*, 421–427.
76. Mertz, C.J.; Kaminski, M.D.; Xie, Y.; Finck, M.R.; Guy, S.; Rosengart, A.J. *In vitro* studies of functionalized magnetic nanospheres for selective removal of a simulant biotoxin. *J. Magn. Magn. Mater.* **2005**, *293*, 572–577.
77. Mikhaylova, M.; Jo, Y.; Kim, D.; Bobrysheva, N.; Andersson, Y.; Eriksson, T.; Osmolowsky, M.; Semenov, V.; Muhammed, M. The Effect of Biocompatible Coating Layers on Magnetic Properties of Superparamagnetic Iron Oxide Nanoparticles. *Hyperfine Interact.* **2004**, *156–157*, 257–263.
78. Qiu, X.P.; Winnik, F. Preparation and characterization of PVA coated magnetic nanoparticles. *Chin. J. Polym. Sci.* **2000**, *18*, 535–539.
79. Yiu, H.H.P.; Wright, P.A.; Botting, N.P. Enzyme immobilisation using SBA-15 mesoporous molecular sieves with functionalised surfaces. *J. Mol. Catal. B: Enzym.* **2001**, *15*, 81–92.
80. Ameur, S.; Martelet, C.; Jaffrezic-Renault, N.; Chovelon, J.-M. Sensitive immunodetection through impedance measurements onto gold functionalized electrodes. *Appl. Biochem. Biotechnol.* **2000**, *89*, 161–170.
81. Arsianti, M.; Lim, M.; Lou, S.N.; Goon, I.Y.; Marquis, C.P.; Amal, R. Bi-functional gold-coated magnetite composites with improved biocompatibility. *J. Colloid Interface Sci.* **2011**, *354*, 536–545.
82. Williams, D.; Gold, K.; Holoman, T.; Ehrman, S.; Wilson, O. Surface modification of magnetic nanoparticles using gum arabic. *J. Nanopart. Res.* **2006**, *8*, 749–753.
83. Klabunde, K.J.; Stark, J.; Koper, O.; Mohs, C.; Park, D.G.; Decker, S.; Jiang, Y.; Lagadic, I.; Zhang, D. Nanocrystals as stoichiometric reagents with unique surface chemistry. *J. Phys. Chem.* **1996**, *100*, 12142–12153.

84. Zhang, H.; Xia, T.; Meng, H.; Xue, M.; George, S.; Ji, Z.; Wang, X.; Liu, R.; Wang, M.; France, B.; *et al.* Differential expression of syndecan-1 mediates cationic nanoparticle toxicity in undifferentiated versus differentiated normal human bronchial epithelial cells. *ACS Nano* **2011**, *5*, 2756–2769.
85. Sunoqrot, S.; Bae, J.W.; Jin, S.E.; Ryan, M.P.; Liu, Y.; Hong, S. Kinetically controlled cellular interactions of polymer-polymer and polymer-liposome nanohybrid systems. *Bioconjugate Chem.* **2011**, *22*, 466–474.
86. Schweiger, C.; Pietzonka, C.; Heverhagen, J.; Kissel, T. Novel magnetic iron oxide nanoparticles coated with poly(ethylene imine)-g-poly(ethylene glycol) for potential biomedical application: Synthesis, stability, cytotoxicity and MR imaging. *Int. J. Pharm.* **2011**, *408*, 130–137.
87. Boussif, O.; Lezoualc'h, F.; Zanta, M.A.; Mergny, M.D.; Scherman, D.; Demeneix, B.; Behr, J.P. A versatile vector for gene and oligonucleotide transfer into cells in culture and *in vivo*: Polyethylenimine. *Proc. Natl. Acad. Sci. USA* **1995**, *92*, 7297–7301.
88. Thomas, M.; Lu, J.J.; Ge, Q.; Zhang, C.; Chen, J.; Klibanov, A.M. Full deacylation of polyethylenimine dramatically boosts its gene delivery efficiency and specificity to mouse lung. *Proc. Natl. Acad. Sci. USA* **2005**, *102*, 5679–5684.
89. Abdallah, B.; Hassan, A.; Benoist, C.; Goula, D.; Behr, J.P.; Demeneix, B.A. A powerful nonviral vector for *in vivo* gene transfer into the adult mammalian brain: Polyethylenimine. *Hum. Gene Ther.* **1996**, *7*, 1947–1954.
90. Zuo, K.H.; Jiang, D.L.; Zhang, J.X.; Lin, Q.L. Forming nanometer TiO_2 sheets by nonaqueous tape casting. *Ceram. Int.* **2007**, *33*, 477–481.
91. Ieda, M.; Fu, J.D.; Delgado-Olguin, P.; Vedantham, V.; Hayashi, Y.; Bruneau, B.G.; Srivastava, D. Direct reprogramming of fibroblasts into functional cardiomyocytes by defined factors. *Cell* **2010**, *142*, 375–386.
92. Takeuchi, J.K.; Bruneau, B.G. Directed transdifferentiation of mouse mesoderm to heart tissue by defined factors. *Nature* **2009**, *459*, 708–711.
93. Vierbuchen, T.; Ostermeier, A.; Pang, Z.P.; Kokubu, Y.; Sudhof, T.C.; Wernig, M. Direct conversion of fibroblasts to functional neurons by defined factors. *Nature* **2010**, *463*, 1035–1041.
94. Zhou, Q.; Brown, J.; Kanarek, A.; Rajagopal, J.; Melton, D.A. *In vivo* reprogramming of adult pancreatic exocrine cells to beta-cells. *Nature* **2008**, *455*, 627–632.
95. Takahashi, K.; Yamanaka, S. Induction of pluripotent stem cells from mouse embryonic and adult fibroblast cultures by defined factors. *Cell* **2006**, *126*, 663–676.
96. Laurent, N.; Sapet, C.D.; Le Gourrierec, L.; Bertosio, E.; Zelphati, O. Nucleic acid delivery using magnetic nanoparticles: The Magnetofection™ technology. *Ther. Deliv.* **2011**, *2*, 471–482.
97. Sonawane, N.D.; Szoka, F.C., Jr.; Verkman, A.S. Chloride accumulation and swelling in endosomes enhances DNA transfer by polyamine-DNA polyplexes. *J. Biol. Chem.* **2003**, *278*, 44826–44831.
98. Brunner, S.; Sauer, T.; Carotta, S.; Cotten, M.; Saltik, M.; Wagner, E. Cell cycle dependence of gene transfer by lipoplex, polyplex and recombinant adenovirus. *Gene Ther.* **2000**, *7*, 401–407.
99. Nishiyama, N.; Kataoka, K. Current state, achievements, and future prospects of polymeric micelles as nanocarriers for drug and gene delivery. *Pharmacol. Ther.* **2006**, *112*, 630–648.

100. Yu, J.H.; Quan, J.S.; Huang, J.; Nah, J.W.; Cho, C.S. Degradable poly(amino ester) based on poly(ethylene glycol) dimethacrylate and polyethylenimine as a gene carrier: Molecular weight of PEI affects transfection efficiency. *J. Mater. Sci.: Mater. Med.* **2009**, *20*, 2501–2510.
101. Veiseh, O.; Kievit, F.M.; Gunn, J.W.; Ratner, B.D.; Zhang, M. A ligand-mediated nanovector for targeted gene delivery and transfection in cancer cells. *Biomaterials* **2009**, *30*, 649–657.
102. Pan, X.; Guan, J.; Yoo, J.W.; Epstein, A.J.; Lee, L.J.; Lee, R.J. Cationic lipid-coated magnetic nanoparticles associated with transferrin for gene delivery. *Int. J. Pharm.* **2008**, *358*, 263–270.
103. Li, Z.; Xiang, J.; Zhang, W.; Fan, S.; Wu, M.; Li, X.; Li, G. Nanoparticle delivery of anti-metastatic NM23-H1 gene improves chemotherapy in a mouse tumor model. *Cancer Gene Ther.* **2009**, *16*, 423–429.
104. Gonzalez, B.; Ruiz-Hernandez, E.; Feito, M.J.; Lopez de Laorden, C.; Arcos, D.; Ramirez-Santillan, C.; Matesanz, C.; Portoles, M.T.; Vallet-Regi, M. Covalently bonded dendrimer-maghemite nanosystems: Nonviral vectors for *in vitro* gene magnetofection. *J. Mater. Chem.* **2011**, *21*, 4598–4604.
105. Wu, H.-C.; Wang, T.-W.; Bohn, M.C.; Lin, F.-H.; Spector, M. Novel magnetic hydroxyapatite nanoparticles as non-viral vectors for the glial cell line-derived neurotrophic factor Gene. *Adv. Funct. Mater.* **2010**, *20*, 67–77.
106. Zhao, D.; Gong, T.; Zhu, D.; Zhang, Z.; Sun, X. Comprehensive comparison of two new biodegradable gene carriers. *Int. J. Pharm.* **2011**, in press.
107. Kami, D.; Takeda, S.; Makino, H.; Toyoda, M.; Itakura, Y.; Gojo, S.; Kyo, S.; Umezawa, A.; Watanabe, M. Efficient transfection method using deacylated polyethylenimine-coated magnetic nanoparticles. *J. Artif. Organs* **2011**, in press.
108. Moghimi, S.M.; Symonds, P.; Murray, J.C.; Hunter, A.C.; Debska, G.; Szewczyk, A. A two-stage poly(ethylenimine)-mediated cytotoxicity: Implications for gene transfer/therapy. *Mol. Ther.* **2005**, *11*, 990–995.
109. Zou, S.M.; Erbacher, P.; Remy, J.S.; Behr, J.P. Systemic linear polyethylenimine (L-PEI)-mediated gene delivery in the mouse. *J. Gene Med.* **2000**, *2*, 128–134.
110. Biswas, S.; Gordon, L.E.; Clark, G.J.; Nantz, M.H. Click assembly of magnetic nanovectors for gene delivery. *Biomaterials* **2011**, *32*, 2683–2688.
111. Ahmed, M.; Deng, Z.; Narain, R. Study of transfection efficiencies of cationic glyconanoparticles of different sizes in human cell line. *ACS Appl. Mater. Interfaces* **2009**, *1*, 1980–1987.
112. Frohlich, E.; Kueznik, T.; Samberger, C.; Roblegg, E.; Wrighton, C.; Pieber, T.R. Size-dependent effects of nanoparticles on the activity of cytochrome P450 isoenzymes. *Toxicol. Appl. Pharmacol.* **2010**, *242*, 326–332.
113. McBain, S.C.; Griesenbach, U.; Xenariou, S.; Keramane, A.; Batich, C.D.; Alton, E.W.F.W.; Dobson, J. Magnetic nanoparticles as Gene delivery agents: Enhanced transfection in the presence of oscillating magnet arrays. *Nanotechnology* **2008**, *19*, 405102.
114. Kamau, S.W.; Hassa, P.O.; Steitz, B.; Petri-Fink, A.; Hofmann, H.; Hofmann-Amtenbrink, M.; von Rechenberg, B.; Hottiger, M.O. Enhancement of the efficiency of non-viral gene delivery by application of pulsed magnetic field. *Nucleic Acids Res.* **2006**, *34*, e40.

115. Dimos, J.T.; Rodolfa, K.T.; Niakan, K.K.; Weisenthal, L.M.; Mitsumoto, H.; Chung, W.; Croft, G.F.; Saphier, G.; Leibel, R.; Goland, R.; *et al.* Induced pluripotent stem cells generated from patients with ALS can be differentiated into motor neurons. *Science* **2008**, *321*, 1218–1221.
116. Ebert, A.D.; Yu, J.; Rose, F.F., Jr.; Mattis, V.B.; Lorson, C.L.; Thomson, J.A.; Svendsen, C.N. Induced pluripotent stem cells from a spinal muscular atrophy patient. *Nature* **2009**, *457*, 277–280.
117. Okita, K.; Ichisaka, T.; Yamanaka, S. Generation of germline-competent induced pluripotent stem cells. *Nature* **2007**, *448*, 313–317.
118. Okita, K.; Nakagawa, M.; Hyenjong, H.; Ichisaka, T.; Yamanaka, S. Generation of mouse induced pluripotent stem cells without viral vectors. *Science* **2008**, *322*, 949–953.
119. Takahashi, K.; Tanabe, K.; Ohnuki, M.; Narita, M.; Ichisaka, T.; Tomoda, K.; Yamanaka, S. Induction of pluripotent stem cells from adult human fibroblasts by defined factors. *Cell* **2007**, *131*, 861–782.

Cancer
Science & Therapy

Kurioka et al. J Cancer Sci Ther 2011, 3:3
http://dx.doi.org/10.4172/1948-5956.1000059

Review Article Open Access

Multicellular Spheroid Culture Models: Applications in Prostate Cancer Research and Therapeutics

Daisuke Kurioka[1], Akimitsu Takagi[2], Misao Yoneda[3], Yoshifumi Hirokawa[3], Taizo Shiraishi[3] and Masatoshi Watanabe[1]*

[1]*Laboratory for Medical Engineering, Division of Materials Science and Chemical Engineering, Graduate School of Engineering, Yokohama National University, Yokohama, Japan*
[2]*Yakult Central Institute for Microbiological Research, Tokyo, Japan*
[3]*Department of Pathologic Oncology, Institute of Molecular and Experimental Medicine, Mie University Graduate School of Medicine, Tsu, Japan*

Abstract

Prostate cancer is one of the most prevalent cancers in men in Western countries, increasing in frequency with age through the most advanced years. Patients with localized prostate cancer are generally treated with radical prostectomy or radiation therapy. However, treatment of more malignant stages of the disease is problematic. Docetaxel-based chemotherapy in men with androgen-independent prostate cancer has been shown to have survival benefits but hormonal manipulation and other chemotherapeutic regimens, especially for androgen-independent lesions, have uncertain value. While research into the complex pathophysiology of advanced prostate cancer has led to identification of mechanisms and target molecules, it nevertheless remains necessary to develop new anticancer drugs. Cell culture models that mimic the structure and features of prostate cancer *in vivo* are necessary for research on tumor biology and design of novel anticancer therapies. In this context, 3-dimensional cultures of prostate cancer cells, including multicellular spheroid (MCS) cultures, started attracting increasing attention.

The present review provides up-to-date information regarding the significance of MCS culture for identification of mechanisms underlying human malignancies, including prostate cancer, and possible targets for prostate cancer therapies.

Keywords: Multicellular spheroid (MCS); Prostate cancer; Drug resistance; Epigenetics; Poly (ADP-ribose) polymerase 1 (PARP-1)

Introduction

Prostate cancer is the most common cancer in men from Western countries, and in particular from the United States of America [1]. Incidences and mortality rates of prostate cancer vary greatly among different geographic areas and ethnic groups. In Japan, the incidence is still low compared with Western countries. However, figures are increasing [2]. Thus, Prostate cancer is the most common cancer in men in Western countries , this place having been occupied by stomach cancer in 1995 [3]. Most patients present with clinically localized disease at the time of diagnosis, and prostate-specific antigen (PSA) and transrectal ultrasound are used to aid in biopsy. Several management options are available when prostate cancer is diagnosed at an early stage, including surgery, cryosurgery, radiation therapy, hormonal therapy, and watchful waiting. For advanced prostate cancers, surgical or medical ablation of androgens is regarded as the optimal first-line treatment [4]. In most patients treated with androgen deprivation, however, disease progression will occur and result in a stage referred to as hormone-refractory prostate cancer. Development of such hormone-refractory state involves a complex series of events such as selection and outgrowth of preexisting clones of androgen-independent cells, adaptive up-regulation of genes that contribute to cancer cell survival and growth after androgen ablation [5]. However, this process is not yet entirely understood.

Patients with hormone-refractory prostate cancer (HRPC) require new agents. Two trials with docetaxel-based chemotherapy demonstrated a significant improvement in overall survival, disease-free survival, pain control, and PSA response [6,7]. Therefore, the United States Food and Drug Administration (FDA) has recommended 3-weekly docetaxel with prednisone as the first-line regimen for patients with HRPC. Despite the benefits, survival remains short and most patients actually do not benefit from docetaxel-based chemotherapy. Effective second- and third-line treatments are still urgently needed and emerging new drugs clearly require evaluation. Although the effects of several anticancer drugs for prostate cancer have been evaluated *in vitro* and in animal experiments, most have had little or no impact on the survival of patients with HRPC and metastatic prostate cancer [8]. One of the reasons for discrepancies between *in vivo* and *in vitro* experiments is thought to be the disordered arrangement of cells within the tumor tissue, in clear contrast to the ordered arrangement in 2-dimensional (2D) cultures [9,10]. Thus, preclinical experimental models mimicking the clinical characteristics of prostate cancer are a high priority for testing new agents against prostate cancer. This review covers up-to-date information regarding the significance of 3-dimensional (3D) culture models, especially multicellular spheroid (MCS) culture models for identification of mechanisms in prostate cancer and target molecules for therapy.

Three-dimensional culture models to study tumor biology

The mechanism of drug resistance is associated with overexpression of P-glycoprotein (P-gp), a protein efflux pump. Multicellular resistance (MCR), which emerges as soon as cells have established contact with their microenvironment, is also involved [11]. The development of methods to clarify the mechanisms of tumor microenvironment–mediated drug resistance is clearly important. Two-dimensional culture models have been used widely as *in vitro* models for drug discovery in the field of cancer biology. They are easy and convenient to set up but lack tumor tissue features like tumor cell–tumor cell, tumor cell–stromal cell, and tumor cell–extracellular matrix (ECM) interactions as well as its typical structural architecture. Cancer cells are also labile, and their behavior can be modulated by the extracellular microenvironment and culture conditions. Comparison between the gene expression patterns of tumor tissues and immortalized cell lines has highlighted some transcriptional modifications in response to the *in vitro* environment [12-14]. Proteome analysis of 3D compared with 2D colon cancer cell cultures revealed a panel of alterations that may affect a wide variety of cellular functions related to protein synthesis, proliferation, regulation of the cytoskeleton, and apoptosis [15]. In 2D culture models, genes associated with cell cycling, metabolism, and turnover of macromolecules are up-regulated, showing that tumor cells adapt to growth needs and respond to growth factors in the culture medium [12,16,17]. On the other hand, tumor cells repress the expression of genes that may limit their growth potential or that are not necessary for *in vitro* growth. Thus, the value of 2D culture models for cancer research is limited. Importantly, it needs to be stressed that animal test systems are indispensable for pharmacokinetic and toxicological evaluation of candidate therapeutic compounds. However, the number of animal models used in the initial discovery of lead compounds has already begun to decline because of ethical and economic concerns, as well as inaccuracy for predicting clinical efficacy. The same is expected to happen with regard to target validation [18].

Some 3D culture models may satisfy the demands comparatively well and are thus promising tools for anticancer drug screening [19]. Notably, MCS can be cocultured with immune cells to evaluate the efficacy of immunotherapy, which progresses to future-oriented culture models [20]. The 3D culture models known at present are listed in (Table 1).

MCS culture models of prostate cancer cells

MCS culture is a 3D culture technique that closely mimics the tumor microenvironment. As for the case of other malignancies, MCS culture models of prostate cancer cells have been used to study prostate tumor biology, tumor cell–stromal cell interactions, and tumor cell responses to therapy [13,21-40] Recently, a comprehensive panel of spheroid culture models, including normal epithelial cells, their derivatives, and classical prostate cancer cell lines, has been reported [41]. As for MCS culture methods, spontaneous aggregation, liquid overlay, spinner flask, and rotating-wall vessel models have been used. Liquid overlay cultures exhibit enhanced functions relative to 2D cultures [23,25,31]. We have used round-bottomed plates coated with poly (2-hydroxyethyl methacrylate) (poly-HEMA; Sigma. Inc., St. Louis, MO) to monitor and manipulate arranged single spheroids at particular growth stages. Under some culture conditions, MCS of prostate cancer cell lines appear to be induced through enhanced expression of E-cadherin. PC-3 (human prostate cancer cell line) cells exhibiting abnormal E-cadherin–mediated cell–cell adhesion are unable to form compact spheroids or tight aggregates, yet loose aggregation in a liquid overlay culture has been reported [13,23,25-31,42]. Moreover, treatment with an anti–E-cadherin antibody inhibits spheroid formation of DU-145 (human prostate carcinoma, epithelial-like cell line) and LNCaP (human prostate adenocarcinoma cell line) cells (Figure1). Besides its function in the formation of MCS, E-cadherin plays an important role in suppression of anoikis [43]. Aggregation of PC-3 cells rather than MCS formation occurs on agar- or poly-HEMA–coated plates; on Matrigel, a one-cell-thick spheroid is formed that partially induces normal differentiation of PC-3 cells [23,25,28]. These findings suggest that MCS formation may be dependent on tumor cell adhesion molecules and culture conditions. In addition, different MCS formation techniques may lead to different MCS phenotypes with different gene expression patterns [44]. Thus, it is essential to carefully select the most appropriate method.

Model	Method	Description
Multicellular spheroid		Spherical aggregate of cells in static or stirred suspension culture
	Spontaneous aggregation Liquid-overlay	A small number of cell types forms clusters rather than strict spheroids Cells cultured on the surface of an agarose gel matrix which blocks attachment of the cells
	Microcarrier beads	Beads support aggregation of attached dependent cells to form pseudo-spheroids in gyratory and spinner flasks
	Spinner flask	Greater quantities of spheroids can be cultivated in suspension than in liquid-overlay cultures
	Gyratory shaker	Cell suspensions in Erlenmeyer flasks containing a specific amount of medium are rotated in a gyratory rotation incubator
	Rotary cell culture	The low shear environment provides an advantage over static and stirred cultures, allowing cells to aggregate, grow like 3D structure and differentiate
Cellular multilayer		Layers of cells cultured on top of a porous membrane
Scaffold-based culture		Cells cultured in synthetic 3D-simulating matrices
Hollow-fiber bioreactor		Cells cultured within a network of perfused artificial capillaries

Table 1: Summary of three-dimensional culture models [16,18].

DU-145 cells form fused compact spheroids, and both DU-145 and LNCaP cells grow at significantly slower rates than in 2D culture [23,25]. MCS of LNCaP cells exhibit disordered but tight cell–cell contacts, and their characteristics differ according to the location [13]. In two studies, the tumor cells of the intermediate zone were found to be positive for p27 and poly (ADP-ribose) polymerase 1 (PARP-1), but negative for Ki-67 (Figure 2a) [13,45]. These cells thus appear to be quiescent. All in all, the structure of a MCS is heterogeneous, with proliferating cells at the periphery and necrotic cells at the center [10,13]. Quiescent cells are viable but remain in a reversible state of growth arrest. The mechanism of their development within MCS remains unclear but appears to be a consequence of microenvironmental factors such as deprivation of growth factors and/or nutrients [10,13,46]. In general, slow-growing tumors tend to be more drug- or ionizing radiation–resistant than rapidly growing tumors. There is no indication as to whether the proportion of quiescent cells is higher in MCS [11]. However, the presence and proportion of quiescent cells may be important determinants of the efficacy of chemotherapy

Differential expression of p18INK4c, p21waf1/cip1, and p27kip1 with respect to their location in the spheroids of EMT6 (mouse mammary tumor cell line) and MEL28 (human melanoma cell line) cells has also been reported: p21waf1/cip1 is found in the outer, proliferating cells, whereas p18INK4c and p27kip1 expression becomes elevated with increasing depth [47]. A decrease in all cell cycle regulatory proteins such as cyclin-dependent kinases (CDKs), CDK inhibitors (CKIs), and cyclins in the innermost spheroid fraction has also been observed [47]. These findings suggest molecular regulation of cell cycle progression in the inner region of spheroids due to microenvironmental stress and hypoxia, which evokes cell cycle arrest via the cyclin-dependent kinase inhibitor p27kip1 [48]. Quiescence was found due to marked

***Corresponding author:** Masatoshi Watanabe, M.D., Ph.D. Laboratory for Medical Engineering, Division of Materials Science and Chemical, Engineering, Graduate School of Engineering, Yokohama National University, 79-5 Tokiwadai, Hodogayaku, Yokohama, Japan; E-mail: mawata@ynu.ac.jp

Received November 06, 2010; **Accepted** January 26, 2011; **Published** February 04, 2011

Citation: Kurioka D, Takagi A, Yoneda M, Hirokawa Y, Shiraishi T, et al. (2011) Multicellular Spheroid Culture Models: Applications in prostate Cancer Research and Therapeutics. J Cancer Sci Ther 3: 060-065. doi:10.4172/1948-5956.1000059

Citation: Kurioka D, Takagi A, Yoneda M, Hirokawa Y, Shiraishi T, et al. (2011) Multicellular Spheroid Culture Models: Applications in prostate Cancer Research and Therapeutics. J Cancer Sci Ther 3: 060-065. doi:10.4172/1948-5956.1000059

cell contact–dependent up-regulation of p27kip1 in EMT6 spheroids, leading to drug or radiation resistance [49,50]. Ki-67 is a nuclear protein expressed during all active phases of the cell cycle. Therefore, it is expressed in proliferating but not in quiescent cells [10,13,46]. In contrast, a dramatic increase of p27kip1 was detected in every cell of the MCS in response to serum withdrawal, which is thought to be a specific environment [46]. In addition, up-regulation of P-gp in G0/G1-phase cells requires expression of p27kip1 but not of p21waf1, suggesting that, under stress conditions (for instance, in hypoxia), p27kip1 contributes to a cell cycle arrest that is essential for cell survival, whereas P-gp contributes to cell survival by helping detoxify waste products [51].

PARPs are enzymes present in eukaryotes; these enzymes are involved in cell signaling through poly (ADP-ribosyl) ation of DNA-binding proteins [52,53]. By catalyzing the addition of ADP-ribose units to DNA, histones, and various DNA repair enzymes, they play multifunctional roles in many cellular processes. PARP-1 (EC 2.4.2.30) was the first of this family to be described in association with cellular responses to DNA damage [52,53]. PARP-1 has a critical role in the repair of DNA single-strand breaks (SSB) through excision repair pathway. In addition, PARP-1 binds to DNA double-strand breaks (DSB) and activates several proteins involved in homologous recombination repair and nonhomologous end-joining pathways. Besides being involved in DNA repair, PARP can also act as a mediator of cell death [53]. Extensive DNA damage is known to trigger PARP overactivation with consequent extensive NAD consumption through ADP-ribose polymer synthesis, leading to ATP depletion and induction of necrosis.

In human malignancies, increased expression of PARP-1 has been reported in Ewing's sarcomas and in malignant lymphomas; conversely, decreased PARP-1 expression has been found in breast cancer and several other cell lines [53]. High PARP expression in prostate cancer cell lines compared to benign cell lines has already been reported, in which greater than 90% of LNCaP cells showed positivity for PARP before and after treatment with H2O2 [54]. In LNCaP spheroids, expression of PARP-1 was detected and confined to the intermediate zone (Figure 2a) [37,45], but real-time PCR demonstrated that expression of PARP-1 in 2D cultures is higher than in spheroid cultures. The specific location means that PARP maycontribute to the characteristics of the quiescent cells within the LNCaP spheroids, being linked with the target molecule in prostate cancer treatments. However, [55] reported that in glioma spheroids, PARP expression, which is initially diffuse, becomes confined to the outer proliferative zone, paralleling the expression of Ki-67. The authors speculated that this phenomenon might be consistent with a role for PARP in cell proliferation and determination of the biological behavior of gliomas.

Epigenetic mechanisms that can affect gene expression without altering the actual sequence of DNA include DNA methylation,

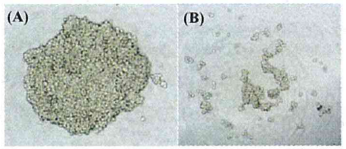

Figure 1: Role of E-cadherin in the formation of a LNCaP spheroid. (A) LNCaP cells form spheroids when cultured on poly-HEMA-coated dishes. (B) Treatment with an anti- E-cadherin antibody (HECD-1) inhibits LNCaP spheroid formation (Takagi et al., unpublished data).

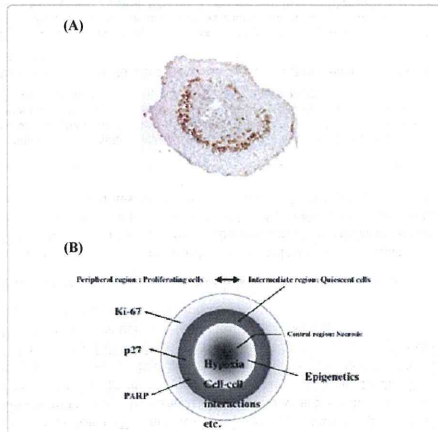

Figure 2: Localization of PARP-1 in a LNCaP spheroid and structure of a multicellular spheroid (MCS). (A) A section of a 7-day spheroid was stained with an anti-PARP-1 antibody (A6.4.12; Serotec, Oxford, UK). There is the intermediate zone with PARP immunostaining. (B) Structure of a MCS and characteristics of the tumor microenvironment. The structure of the spheroid favors genetic and epigenetic alterations.

RNA-associated silencing, and histone modification. These phenomena importantly affect gene expression during development [56]. Methylation of the C5 position of cytosine residues in DNA is recognized as a particularly important epigenetic silencing mechanism. Histone modification is another important epigenetic mechanism that determines their interactions with other proteins, thereby regulating chromatin structure and remodeling. DNA methylation and histone modifications related to chromatin remodeling have been intensively analyzed in various tumor types [57]. Thus, it is interesting to examine the epigenetic state of cancer cells in spheroids. [58] found that, similar to spheroids, TSUPr1 cells dynamically change their methylation patterns and the expression of E-cadherin as a function of the cellular microenvironment. They distinctively speculated that the cellular microenvironment selects for cells that have an appropriate methylation pattern, and that spheroid formation may increase the transcriptional expression E-cadherin, which in turn may drive regional hypomethylation of densely methylated CpG islands. This finding is very interesting because a methylation-regulated gene in a spheroid culture changes within a few days as compared to 2D cultures. A recent study by [59] has shown that increased levels of heterochromatin in spheroids characterized by histone H3 deacetylation and increased heterochromatin protein 1α expression result in improved radiation survival and reduced numbers of DNA DSBs and lethal chromosome aberrations. A previous report showed that 3D growth of mammary epithelial cells reduced histone H3 and H4 acetylation and gene expression, although ECM-controlled cell shape was discussed [60]. Few studies about DNA methylation in spheroids have been reported. Similarly, little is known about the action of DNA methyltransferase (DNMT) enzymes. However, preliminary data showed that there are no significant differences in long interspersed nucleotide element 1 (LINE-1) hypomethylation between 2D culture and MCS of LNCaP cells [37].

Citation: Kurioka D, Takagi A, Yoneda M, Hirokawa Y, Shiraishi T, et al. (2011) Multicellular Spheroid Culture Models: Applications in prostate Cancer Research and Therapeutics. J Cancer Sci Ther 3: 060-065. doi:10.4172/1948-5956.1000059

The microenvironment of solid tumors such as prostate cancer is characterized by hypoxia, low extracellular pH, and nutrient deprivation. Under hypoxia, tumor cells increase expression of various genes, for instance those contributing to angiogenesis, partially through hypoxia-induced factor 1 (HIF-1). On the other hand, genes involved in cellular adhesion and DNA repair are decreased [61]. Down-regulation of mutL homologue 1 (MLH-1) in 2D cultures of EMT-6 cells under hypoxic conditions has been detected, with PM2 expression being unchanged [62]. However, down-regulation of PM2 was detected in EMT-6 spheroids. These results suggest that tumors can down-regulate DNA mismatch repair as a result of a series of microenvironmental factors, which results in increased resistance to alkylating agents. It has been hypothesized that hypoxia may influence local epigenetic alterations, leading to inappropriate silencing and reawakening of cancer genes [63]. A reduction of 5-methylcytosine in xenografts compared to the levels in the same cancer cell lines *in vitro* has been reported, providing direct evidence that epigenetic events in solid tumors may be modulated by microenvironmental stress [64]. In several mammalian cell lines, hypoxia increases globaldimethylated histone H3 lysine 9 (H3K9me2) expression through histone methyltransferase G9a, leading to inhibition of gene expression [64].

These findings suggest that epigenetic alterations in spheroids may be linked to their microenvironment. Whether activation or stimulation of anticancer drug resistance–related genes such as MDR-1 is brought about by epigenetic events is an intriguing possibility that needs to be analyzed.

Applications to prostate cancer therapy

Like solid tumors in vivo, MCS is characterized by hypoxic regions, The presence of hypoxic tumor microenvironment correlates with increased tumor invasiveness, metastases, and resistance to chemotherapy and radiotherapy [65]. Chemotherapeutic drug resistance in cancer cells under hypoxia is partially caused by reduced toxicity because of the absence of molecular oxygen. Hypoxia and nutrient deprivation can also promote mitochondrial reactive oxygen species (ROS) production, which result in modulation of ROS levels and energy metabolism to activate many signalling pathways leading to HIF family protein stabilization and activation [66]. Chemotherapeutic drug resistance is caused by HIF family–induced inhibition of cell cycle progression and proliferation.

Androgen ablation leads to an initial favorable response in patients. However, most relapse with an aggressive form of the disease known as castration-resistantor hormone-refractory prostate cancer. As critical molecular events that lead to prostate cancer cell resistance to androgen-deprivation therapy have been reported, there is also a possibility that hypoxia may be involved in the transition to androgen independence. Crosstalk between the androgen receptor and HIF-1α in prostate cancer cells has been reported [67]. Thus, methods of targeting the microenvironment, especially hypoxia, have been investigated, e.g., to increase the oxygen supply to the tumor hypoxic area, to exploit the microenvironment by using bioreductive drugs, and to exploit the biological response to hypoxia by targeting HIF-1α.

PARP has attracted considerable attention as a therapeutic target for various diseases including cancer. Enhanced PARP-1 expression and/or its activity has been shown in several tumor cell lines, contributing to resistance to genotoxic stress and ability to survive exposure to DNA-damaging agents [52,53]. Inhibition of PARP-1 thus enhances the efficiency of alkylating agents and ionizing radiation [53]. These results have stimulated the development of specific PARP-1 inhibitors as potential chemoand radiosensitizers. Several small-molecule PARP inhibitors have indeed been synthesized and introduced into the clinic for treatment of cancer patients [53]. Research into breast cancer 2 susceptibility protein (BRCA2)-deficient cells, which are highly sensitive to inhibitors of PARP, has provided the basis for new therapeutic approaches [53]. Recently, a PARP inhibitor has been reported to radiosensitize DU-145 cells under hypoxia [68]. Like PARP, other proteins expressed by quiescent cells in MCSs may constitute targets for prostate cancer therapy.

The cancer stem cell (CSC) theory has emerged as a paradigm shift in our understanding of cancer as a disease of stem cells. A small subset of cancer cells within the tumor mass has the exclusive capacity to divide and expand the CSC pool and to differentiate into nontumorigenic, more differentiated cancer cell lineages. The existence of these small subsets of cells is responsible for tumor recurrence and metastasis. Thus, effective therapeutics should target rare CSCs that sustain tumor malignancy [69]. Such small subsets have been detected not only in malignancies of the blood but also in solid tumors in the brain, breast, and prostate, among others. Recent studies with prostate cells have also shown that nonmalignant immortalized cell lines and malignant cell lines contain a subset of cells with stem cell properties. In the spheroid culture system, nonmalignant and malignant human hTERT-immortalized prostate epithelial cells have been reported to maintain high CD133 expression [70]. The spheroid culture methods appear to contribute to the identification of CSCs from the prostate, which may be a new target for prostate cancer therapy.

Summary

MCS culture models have become a mainstream culture model for tumor biology and identification of anticancer resistance mechanisms as an alternative to the classical 2D culture models that poorly reflect the structural characteristicsseen in vivo. MCS culture models better mimic the growth characteristics of in vivo solid tumors. Like other solid tumors, prostate cancer creates a microenvironment characterized by hypoxia, acidosis, and nutrient deprivation, which collectively lead to tumor genetic and adaptive changes (Figure 2b). The tumor microenvironment correlates with prostate cancer invasiveness, metastasis, and resistance to radiotherapy and chemotherapy. Hypoxia may also be involved in the transition of prostate cancer to androgen independence. MCS culture models are a good model for understanding the mechanisms of resistance to chemotherapy, radiotherapy, and androgen ablation, and discovery of new targets for prostate cancer, especially androgen-independent cancer. Our review has highlighted the characteristics of prostate cancer MCS (p27 and PARP expression, and epigenetics), and underlined the tumor microenvironment as target for prostate cancer therapy. MCS culture models appear to contribute to the identification of CSCs from the prostate.

Further studies are needed to clarify mechanisms such as epigenetic regulation, to better characterize the formation of MCS, and to apply this knowledge into prostate cancer biology and the discovery of new targets for prostate cancer.

Acknowledgments

This work was supported in part by a Grant-in-Aid for Scientific Research from the Ministry of Education, Culture, Sports, Science and Technology, and a Grant-in-Aid from the Yokohama National University Global COE Program.

References

1. Jemal A, Siegel R, Ward E, Hao Y, Xu J, et al. (2008) Cancer statistics, 2008. CA Cancer J Clin 58: 71-96.
2. Watanabe M, Nakayama T, Shiraishi T, Stemmermann GN, Yatani R (2000) Comparative studies of prostate cancer in Japan versus the United States: A review. Urol Oncol 5: 274-283.

3. Tabata N, Ohno Y, Matsui R, Sugiyama H, Ito Y, et al. (2008) Partial cancer prevalence in Japan up to 2020: estimates based on incidence and survival data from population-based cancer registries. Jpn J Clin Oncol 38: 146-157.
4. Bhandari MS, Petrylak DP, Hussain M (2005) Clinical trials in metastatic prostate cancer-has there been real progress in the past decade? Eur J Cancer 41: 941-953.
5. So A, Gleave M, Hurtado-Col A, Nelson C (2005) Mechanisms of the development of androgen independence in prostate cancer. World J Urol 23: 1-9.
6. Petrylak DP, Tangen CM, Hussain MH, Lara PN Jr, Jones JA, et al. (2004) Docetaxel and estramustine compared with mitoxantrone and prednisone for advanced refractory prostate cancer. N Engl J Med 351: 1513-1520.
7. Tannock IF, de Wit R, Berry WR, Horti J, Pluzanska A, et al. (2004) Docetaxel plus prednisone or mitoxantrone plus prednisone for advanced prostate cancer. N Engl J Med 351: 1502-1512.
8. Diaz M, Patterson SG (2004) Management of androgen-independent prostate cancer. Cancer Control 11: 364-373.
9. Sutherland RM, McCredie JA, Inch WR (1971) Growth of multicell spheroids in tissue culture as a model of nodular carcinomas. J Natl Cancer Inst 46: 113-120.
10. Hirschhaeuser F, Menne H, Dittfeld C, West J, Mueller-Klieser W, et al. (2010) Multicellular tumor spheroids: an underestimated tool is catching up again. J Biotechnol 148: 3-15.
11. Desoize B, Jardillier J (2000) Multicellular resistance: a paradigm for clinical resistance? Crit Rev Oncol Hematol 36: 193-207.
12. Birgersdotter A, Sandberg R, Ernberg I (2005) Gene expression perturbation in vitro--a growing case for three-dimensional (3D) culture systems. Semin Cancer Biol 15: 405-412.
13. Takagi A, Watanabe M, Ishii Y, Morita J, Hirokawa Y, Matsuzaki T, et al. (2007) Three-dimensional cellular spheroid formation provides human prostate tumor cells with tissue-like features. Anticancer Res 27: 45-53.
14. De Witt Hamer PC, Van Tilborg AA, Eijk PP, Sminia P, Troost D, et al. (2008) The genomic profile of human malignant glioma is altered early in primary cell culture and preserved in spheroids. Oncogene 27: 2091-2096.
15. Gaedtke L, Thoenes L, Culmsee C, Mayer B, Wagner E (2007) Proteomic analysis reveals differences in protein expression in spheroid versus monolayer cultures of low-passage colon carcinoma cells. J Proteome Res 6: 4111-4118.
16. Kim JB (2005) Three-dimensional tissue culture models in cancer biology. Semin Cancer Biol 15: 365-377.
17. Rodríguez-Enríquez S, Gallardo-Pérez JC, Avilés-Salas A, Marín-Hernández A, Carreño-Fuentes L, et al. (2008) Energy metabolism transition in multi-cellular human tumor spheroids. J Cell Physiol 216: 189-197.
18. Kunz-Schughart LA, Freyer JP, Hofstaedter F, Ebner R (2004) The use of 3-D cultures for high-throughput screening: the multicellular spheroid model. J Biomol Screen 9: 273-285.
19. Burdett E, Kasper FK, Mikos AG, Ludwig JA (2010) Engineering tumors: a tissue engineering perspective in cancer biology. Tissue Eng Part B Rev 16: 351-359.
20. Gottfried E, Kunz-Schughart LA, Andreesen R, Kreutz M (2006) Brave little world: spheroids as an in vitro model to study tumor-immune-cell interactions. Cell Cycle 5: 691-695.
21. Donaldson JT, Tucker JA, Keane TE, Walther PJ, Webb KS (1990) Characterization of a new model of human prostatic cancer: the multicellular tumor spheroid. Int J Cancer 46: 238-244.
22. Ingram M, Techy GB, Saroufeem R, Yazan O, Narayan KS, et al. (1997) Three-dimensional growth patterns of various human tumor cell lines in simulated microgravity of a NASA bioreactor. In Vitro Cell Dev Biol Anim 33: 459-466.
23. Hedlund TE, Duke RC, Miller GJ (1999) Three-dimensional spheroid cultures of human prostate cancer cell lines. Prostate 41: 154-165.
24. O'Connor KC (1999) Three-dimensional cultures of prostatic cells: tissue models for the development of novel anti-cancer therapies. Pharm Res 16: 486-493.
25. Frankel A, Man S, Elliott P, Adams J, Kerbel RS (2000) Lack of multicellular drug resistance observed in human ovarian and prostate carcinoma treated with the proteasome inhibitor PS-341. Clin Cancer Res 6: 3719-3728.
26. Clejan S, O'Connor K, Rosensweig N (2001) Tri-dimensional prostate cell cultures in simulated microgravity and induced changes in lipid second messengers and signal transduction. J Cell Mol Med 5: 60-73.
27. Enmon RM Jr, O'Connor KC, Lacks DJ, Schwartz DK, Dotson RS (2001) Dynamics of spheroid self-assembly in liquid-overlay culture of DU 145 human prostate cancer cells. Biotechnol Bioeng 72: 579-591.
28. Lang SH, Stark M, Collins A, Paul AB, Stower MJ, Maitland NJ (2001) Experimental prostate epithelial morphogenesis in response to stroma and three-dimensional Matrigel culture. Cell Growth Differ 12: 631-640.
29. Enmon RM Jr, O'Connor KC, Song H, Lacks DJ, Schwartz DK (2002) Aggregation kinetics of well and poorly differentiated human prostate cancer cells. Biotechnol Bioeng 80: 580-588.
30. Mitrofanova E, Hagan C, Qi J, Seregina T, Link C Jr (2003) Sodium iodide symporter/radioactive iodine system has more efficient antitumor effect in three-dimensional spheroids. Anticancer Res 23: 2397-2404.
31. Khoei S, Goliaei B, Neshasteh-Riz A, Deizadji A (2004) The role of heat shock protein 70 in the thermoresistance of prostate cancer cell line spheroids. FEBS Lett 561: 144-148.
32. Song H, David O, Clejan S, Giordano CL, Pappas-Lebeau H, et al. (2004a) Spatial composition of prostate cancer spheroids in mixed and static cultures. Tissue Eng 10: 1266-1276.
33. Song H, Jain SK, Enmon RM, O'Connor KC (2004b) Restructuring dynamics of DU 145 and LNCaP prostate cancer spheroids. In Vitro Cell Dev Biol Anim 40: 262-267.
34. O'Connor KC, Venczel MZ (2005) Predicting aggregation kinetics of DU 145 prostate cancer cells in liquid-overlay culture. Biotechnol Lett 27: 1663-1668.
35. Wang R, Xu J, Juliette L, Castilleja A, Love J, et al. (2005) Three-dimensional co-culture models to study prostate cancer growth, progression, and metastasis to bone. Semin Cancer Biol 15: 353-64.
36. Jung V, Wullich B, Kamradt J, Stöckle M, Unteregger G (2007) An improved in vitro model to characterize invasive growing cancer cells simultaneously by function and genetic aberrations. Toxicol In Vitro 21: 183-190.
37. Watanabe M, Takagi A (2008) Biological behavior of prostate cancer cells in 3D culture systems. Yakugaku Zasshi 128: 37-44.
38. Pearson JF, Hughes S, Chambers K, Lang SH (2009) Polarized fluid movement and not cell death, creates luminal spaces in adult prostate epithelium. Cell Death Differ 16: 475-482.
39. Chu JH, Yu S, Hayward SW, Chan FL (2009) Development of a three-dimensional culture model of prostatic epithelial cells and its use for the study of epithelial-mesenchymal transition and inhibition of PI3K pathway in prostate cancer. Prostate 69: 428-442.
40. Hsiao AY, Torisawa YS, Tung YC, Sud S, Taichman RS, et al. (2009) Microfluidic system for formation of PC-3 prostate cancer co-culture spheroids. Biomaterials 30: 3020-3027.
41. Härmä V, Virtanen J, Mäkelä R, Happonen A, Mpindi JP, et al. (2010) A comprehensive panel of three-dimensional models for studies of prostate cancer growth, invasion and drug responses. PLoS One 5: e10431.
42. Mitchell S, Abel P, Ware M, Stamp G, Lalani E (2000) Phenotypic and genotypic characterization of commonly used human prostatic cell lines. BJU Int 85: 932-944.
43. Kang HG, Jenabi JM, Zhang J, Keshelava N, Shimada H, et al. (2007) E-cadherin cell-cell adhesion in ewing tumor cells mediates suppression of anoikis through activation of the ErbB4 tyrosine kinase. Cancer Res 67: 3094-3105.
44. Steadman K, Stein WD, Litman T, Yang SX, Abu-Asab M, et al. (2008) PolyHEMA spheroids are an inadequate model for the drug resistance of the intractable solid tumors. Cell Cycle 7: 818-829.
45. Muggia FM, Peters GJ, Landolph JR Jr (2009) XIII International Charles Heidelberger Symposium and 50 Years of Fluoropyrimidines in Cancer Therapy Held on September 6 to 8, 2007 at New York University Cancer Institute, Smilow Conference Center. Mol Cancer Ther 8: 992-999.
46. Mellor HR, Ferguson DJ, Callaghan R (2005) A model of quiescent tumour microregions for evaluating multicellular resistance to chemotherapeutic drugs. Br J Cancer 93: 302-309.
47. LaRue KE, Khalil M, Freyer JP (2004) Microenvironmental regulation of proliferation in multicellular spheroids is mediated through differential expression of cyclin-dependent kinase inhibitors. Cancer Res 64: 1621-1631.
48. Gardner LB, Li Q, Park MS, Flanagan WM, Semenza GL, et al. (2001) Hypoxia inhibits G1/S transition through regulation of p27 expression. J Biol Chem 276: 7919-7926.
49. St Croix B, Florenes VA, Rak JW, Flanagan M, Bhattacharya N, et al. (1996) Impact of the cyclin-dependent kinase inhibitor p27Kip1 on resistance of tumor cells to anticancer agents. Nat Med 2: 1204-1210.
50. St Croix B, Sheehan C, Rak JW, Florenes VA, Slingerland JM, et al. (1998) E-Cadherin-dependent growth suppression is mediated by the cyclin-dependent kinase inhibitor p27(KIP1). J Cell Biol 142: 557-571.
51. Wartenberg M, Fischer K, Hescheler J, Sauer H (2002) Modulation of intrinsic P-glycoprotein expression in multicellular prostate tumor spheroids by cell cycle inhibitors. Biochim Biophys Acta 1589: 49-62.
52. Masutani M, Nozaki T, Nakamoto K, Nakagama H, Suzuki H, Kusuoka, et al. (2000) The response of Parp knockout mice against DNA damaging agents. Mutat Res 462: 159-166.
53. Ratnam K, Low JA (2007) Current development of clinical inhibitors of poly(ADP-ribose) polymerase in oncology. Clin Cancer Res 13: 1383-1388.
54. McNealy T, Frey M, Trojan L, Knoll T, Alken P, et al. (2003) Intrinsic presence of poly (ADP-ribose) is significantly increased in malignant prostate compared to benign prostate cell lines. Anticancer Res 23: 1473-1478.
55. Wharton SB, McNelis U, Bell HS, Whittle IR (2000) Expression of poly(ADP-ribose) polymerase and distribution of poly(ADP-ribosyl)ation in glioblastoma and in a glioma multicellular tumour spheroid model. Neuropathol Appl Neurobiol 26: 528-35.
56. Watanabe M, Takagi A, Matsuzaki T, Kami D, Toyota M, et al. (2006) Knowledge of epigenetic influence for prostate cancer therapy. Curr Cancer Drug Targets 6: 533-551.
57. Sharma S, Kelly TK, Jones PA (2010) Epigenetics in cancer. Carcinogenesis 31: 27-36.
58. Graff JR, Gabrielson E, Fujii H, Baylin SB, Herman JG (2000) Methylation patterns of the E-cadherin 5' CpG island are unstable and reflect the dynamic, heterogeneous loss of E-cadherin expression during metastatic progression. J Biol Chem 275: 2727-2732.
59. Storch K, Eke I, Borgmann K, Krause M, Richter C, et al. (2010) Three-dimensional cell growth confers radioresistance by chromatin density modification. Cancer Res 70: 3925-3934.
60. Le Beyec J, Xu R, Lee SY, Nelson CM, Rizki A, et al. (2007) Cell shape regulates global histone acetylation in human mammary epithelial cells. Exp Cell Res 313: 3066-75.
61. Maynard MA, Ohh M (2007) The role of hypoxia-inducible factors in cancer. Cell Mol Life Sci 64: 2170-2180.
62. Francia G, Green SK, Bocci G, Man S, Emmenegger U, et al. (2005) Down-regulation of DNA mismatch repair proteins in human and murine tumor spheroids: implications for multicellular resistance to alkylating agents. Mol Cancer Ther 4: 1484-1494.
63. Shahrzad S, Bertrand K, Minhas K, Coomber BL (2007) Induction of DNA hypomethylation by tumor hypoxia. Epigenetics 2: 119-125.
64. Chen H, Yan Y, Davidson TL, Shinkai Y, Costa M (2006) Hypoxic stress induces dimethylated histone H3 lysine 9 through histone methyltransferase G9a in mammalian cells. Cancer Res 66: 9009-9016.
65. Wouters BG, Weppler SA, Koritzinsky M, Landuyt W, Nuyts S, et al. (2002) Hypoxia as a target for combined modality treatments. Eur J Cancer 38: 240-257.
66. Ralph SJ, Rodriguez-Enriquez S, Neuzil J, Saavedra E, Moreno-Sánchez R (2010) The causes of cancer revisited: "mitochondrial malignancy" and ROS-induced oncogenic transformation - why mitochondria are targets for cancer therapy. Mol Aspects Med 31: 145-170.
67. Khandrika L, Kumar B, Koul S, Maroni P, Koul HK (2009) Oxidative stress in prostate cancer. Cancer Lett 282: 125-136.
68. Liu SK, Coackley C, Krause M, Jalali F, Chan N, et al. (2008) A novel poly(ADP-ribose) polymerase inhibitor, ABT-888, radiosensitizes malignant human cell lines under hypoxia. Radiother Oncol 88: 258-268.
69. Rappa G, Mercapide J, Anzanello F, Prasmickaite L, Xi Y, et al. (2008) Growth of cancer cell lines under stem cell-like conditions has the potential to unveil therapeutic targets. Exp Cell Res 314: 2110-2122.
70. Miki J, Rhim JS (2008) Prostate cell cultures as in vitro models for the study of normal stem cells and cancer stem cells. Prostate Cancer Prostatic Dis 11:32-39.

Citation: Kurioka D, Takagi A, Yoneda M, Hirokawa Y, Shiraishi T, et al. (2011) Multicellular Spheroid Culture Models: Applications in prostate Cancer Research and Therapeutics. J Cancer Sci Ther 3: 060-065. doi:10.4172/1948-5956.1000059

J Cancer Sci Ther
ISSN:1948-5956 JCST, an open access journal

J Artif Organs
DOI 10.1007/s10047-011-0568-6

ORIGINAL ARTICLE

Efficient transfection method using deacylated polyethylenimine-coated magnetic nanoparticles

Daisuke Kami · Shogo Takeda · Hatsune Makino · Masashi Toyoda · Yoko Itakura · Satoshi Gojo · Shunei Kyo · Akihiro Umezawa · Masatoshi Watanabe

Received: 6 October 2010 / Accepted: 31 March 2011

Abstract Low efficiencies of nonviral gene vectors, such as transfection reagent, limit their utility in gene therapy. To overcome this disadvantage, we report on the preparation and properties of magnetic nanoparticles [diameter (d) = 121.32 ± 27.36 nm] positively charged by cationic polymer deacylated polyethylenimine (PEI max), which boosts gene delivery efficiency compare with polyethylenimine (PEI), and their use for the forced expression of plasmid delivery by application of a magnetic field. Magnetic nanoparticles were coated with PEI max, which enabled their electrostatic interaction with negatively charged molecules such as plasmid. We successfully transfected 81.1 ± 4.0% of the cells using PEI max-coated magnetic nanoparticles (PEI max-nanoparticles). Along with their superior properties as a DNA delivery vehicle, PEI max-nanoparticles offer to deliver various DNA formulations in addition to traditional methods. Furthermore, efficiency of the gene transfer was not inhibited in the presence of serum in the cells. PEI max-nanoparticles may be a promising gene carrier that has high transfection efficiency as well as low cytotoxicity.

Keywords Deacylated polyethylenimine · Magnetic nanoparticle · Efficient nonviral transfection method

D. Kami
Innovative Integration between Medicine and Engineering Based on Information Communications Technology, Yokohama National University Global COE Program, Yokohama, Japan
e-mail: dkami@tmig.or.jp

S. Takeda · M. Watanabe (✉)
Laboratory for Medical Engineering, Division of Materials and Chemical Engineering, Yokohama National University, 79-1 Tokiwadai, Hodogaya-ku, Yokohama 240-8501, Japan
e-mail: mawata@ynu.ac.jp

D. Kami · H. Makino · M. Toyoda · A. Umezawa
Department of Reproductive Biology, National Institute for Child Health and Development, Tokyo, Japan

D. Kami · M. Toyoda (✉) · Y. Itakura · S. Gojo
Vascular Medicine, Research Team for Geriatric Medicine, Tokyo Metropolitan Institute of Gerontology, 35-2 Sakae-cho, Itabashi-ku, Tokyo 173-0015, Japan
e-mail: mtoyoda@tmig.or.jp

S. Gojo · S. Kyo
Division of Therapeutic Strategy for Heart Failure, Department of Cardio-Thoracic Surgery, The University of Tokyo, Tokyo, Japan

Published online: 03 May 2011

Introduction

Nanotechnologies that allow the nondisruptive introduction of carriers in vivo have wide potential for gene and therapeutic delivery systems [1–4]. Extremely small particles have been successfully introduced into living cells without any further modification to enhance endocytic internalization, such as for cationic help. The cells containing the internalized nanoparticles continued to thrive, indicating that the particles have no inhibitory effect on mitosis. Therefore, iron oxide magnetic nanoparticles have played an important role as magnetic resonance imaging contrast agents [5, 6], and cytotoxicity of this nanoparticle was none (or low) [7, 8]. Thereby, the functionalized iron oxide magnetic nanoparticles are expected to be useful as a new gene delivery tool [3].

Cationic polymer polyethylenimine (PEI) (linear, MW 25,000) is known as the transfection reagent in molecular biology [9], and the dispersant in nanotechnology [10]. PEI are configured to form the positively charged complex with DNA, which binds to anionic cell surface residues and enter the cell via endocytosis [9, 11], keeping the dispersed state in the solution [10]. However, PEI containing residual *N*-acyl groups is a disadvantage for transfection efficiency. Also, the deacylated PEI (PEI max) for transfection reagent was reported, showing an increase in optimal transfection efficiency of 21-fold in comparison with PEI [12].

The transfection method using magnetic nanoparticles utilizes a magnetic force to deliver DNA into target cells. Therefore, the plasmid is first associated with magnetic nanoparticles. Then, the application of a magnetic force drives the plasmid–nanoparticle complexes toward and into the target cells, where the cargo is released (Fig. 1a) [13–16]. The magnetic nanoparticles are also coated with biological polymers, such as PEI, to allow plasmid loading (Fig. 1b). The binding of the negatively charged plasmid to the positively charged PEI max-coated magnetic nanoparticles (PEI max-nanoparticles) occurs relatively quickly. After complex formation, the loaded nanoparticles are incubated together with the target cells on a magnet plate. Owing to the magnetic force, the iron particles are rapidly drawn toward the surface of the cell membrane. Cellular uptake occurs by either endocytosis or pinocytosis [17]. Once delivered to the target cells, the plasmid is released into the cytoplasm [17, 18]. The magnetic nanoparticles accumulate in endosomes and/or vacuoles [18]. Over time, the nanoparticles are degraded and the iron enters normal iron metabolism [19]. An influence of magnetic nanoparticles on cellular functions has not been reported yet. However, in most cases, the increased iron concentration in culture media does not lead to cytotoxic effects [7].

In this study, we coated the transfection reagent, PEI max, on the surface of magnetic nanoparticles and applied a gene vector using PEI max-nanoparticles for a highly efficient transfection method. Our results indicate a high level of expression of the transfected gene in living cells using the plasmid-conjugated PEI max-nanoparticles.

Materials and methods

Materials

Magnetic nanoparticles (γ-Fe_2O_3, d = 70 nm) were purchased from CIK NanoTek. PEI max linear (MW 25,000) was purchased from Polysciences Inc. FuGENE HD was purchased from Roche Diagnostics. Deionized water was purchased from Gibco. Magnetic sheet (160 mT), and neodymium magnet (130 mT) was purchased from Magna Co. Ltd.

Preparation of the PEI max-nanoparticles

The magnetic nanoparticles (1.0 g) were dissolved in 30 ml of PEI max solution (1.6 mg PEI max/ml). The mixture was sonicated for 2 min (40 W) on ice, and 20 ml of deionized water was added (final concentration 1.0 mg PEI max/ml). The ferrofluid was centrifuged at 4,100×g for 5 min. The supernatant fluids were harvested and transferred into a fresh tube. This fluid was washed twice by deionized water and resolved into an equal volume of the PEI max solution (1.0 mg PEI max/ml). Magnetic nanoparticles in this fluid

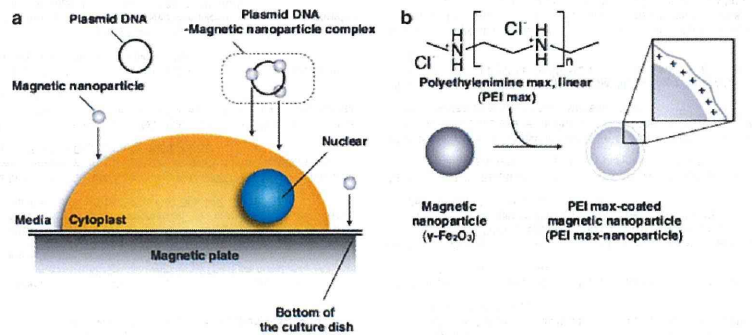

Fig. 1 Nanoparticle transfection method and cationic coating: **a** Plasmid-conjugated magnetic nanoparticles moved to the cell surface on the magnetic sheet upon application of magnetic force. Then, the magnetic force drove this complex toward and into the target cells. **b** Magnetic nanoparticles (γ-Fe_2O_3, d = 70 nm) (CIK NanoTek Inc.) were coated with deacylated polyethylenimine max linear (PEI max) (MW 25,000) (Polysciences Inc.), known as a dispersive agent, and transfection reagents. The surface of the PEI max-nanoparticle was positively charged. Nanoparticles and plasmid formed complexes by ionic interaction of the negatively charged plasmid and the positively charged surface of the PEI max-nanoparticle

were coated with PEI max and dispersed in PEI max solution or deionized water.

Measurement of PEI max-nanoparticle size and ζ-potential

The size of the PEI max-nanoparticles was measured with a laser light-scattering method using a fiberoptics particle analyzer (FPAR-1000, Otsuka Electronics). The measurement was performed in triplicate, and median size and range of size distribution were obtained. The ζ-potential of the PEI max-nanoparticles was determined with electrophoretic light-scattering spectrophotometer (ELSZ-2, Otsuka Electronics).

Charge characteristics of PEI max-nanoparticle

PEI max-nanoparticle (100 μg) and each weight of plasmid (2,000, 1,000, 750, 500, 375, 250, 188 ng) were mixed in deionized water or PEI max solution (1 mg/ml). Each solution were reacted for 1 h at room temperature.

Plasmid DNA was bound to PEI max-nanoparticles

Plasmid DNA (5 μg) was reacted with various weights of PEI max-nanoparticles (0–1.8 mg/tube) in deionized water for 15 min at room temperature. Then, the reaction mixtures were centrifuged at 12,000×*g* for 15 min and were formed in a sol-like precipitation in the lower layer. The concentration of DNA in the upper layer (hyaline layer) was determined by NanoDrop 1000 spectrophotometer (Thermo Scientific). The relative concentration of plasmid DNA treated without PEI max-nanoparticles was regarded as 100%.

Cell culture

P19CL6 cells (CL6 cells) from a mouse embryonic carcinoma cell line were grown on 100-mm dishes (Becton-Dickinson) in alpha-minimum essentioal medium (MEM) (Nacalai Tesque) supplemented with 10% fetal bovine serum (FBS) (JRH Bioscience Inc.), penicillin, and streptomycin (Gibco), and were maintained in a 5% carbon dioxide (CO_2) atmosphere at 37°C.

Transfection procedure using PEI max-nanoparticles

CL6 cells were seeded at 1×10^5 cells/well in six-well plates (Becton-Dickinson) 18 h before transfection. Immediately before transfection, cells were rinsed and supplemented with fresh culture medium (1 ml). The PEI max-nanoparticles (in 1 mg PEI max/ml solution) were mixed with 2.0 μg of the plasmid [pCAGGS–enhanced green fluorescent protein (EGFP), the modified pCAGGS expression vector [20], weight ratio PEI max:plasmid = 3:1] and incubated in the deionized water at final volume of 50 μl at room temperature for 15 min. The complexes were added to the CL6 cells on a magnetic sheet various times (0, 0.5, 1, 4, and 24 h). Forty-eight hours after transfection, CL6 cells were evaluated; 1 mg/ml of PEI max solution was used as a positive control.

Quantitative real-time reverse transcriptional (RT)-PCR

Total RNAs from CL6 cells were extracted using ISOGEN (Nippon Gene). To perform quantitative real-time polymerase chain reaction (PCR) assay, total RNA (1 μg) was reverse-transcribed using random hexamer and the PrimeScript RT reagent kit (TaKaRa). Quantitative real-time reverse transcriptional (RT)-PCR was performed on LineGene (BioFlux), using 100 ng of complementary DNA (cDNA) in 25 μl reaction volumes with 10 nmol/l EGFP primer and 12.5 μl of SYBR Premix Ex Taq (TaKaRa). PCR primers for the gene of EGFP and *Gapdh* were designed to amplify each cDNA using the sense primer (5′-CCGACCACATGAAGCAGCAC-3′) and the reverse primer (5′-CTTCAGCTCGATGCGGTTCAC-3′) for the EGFP, and the sense primer (5′-TGCGACTTCAACAGCA ACTC-3′) and the reverse primer (5′-CTTGCTCAGTGTC CTTGCTG-3′) for the *Gapdh*. Calculations were automatically performed by fluorescent quantitative detection system software (BioFlux).

Nanoparticle cytotoxicity

Alamar Blue [21] was used to measure cell proliferation and metabolic activity as an oxidation-reduction indicator. After 48 h of PEI max or PEI max-nanoparticle exposure, 900 μl of medium from each condition was transferred into a 24-well flat-bottomed plate. One hundred microliters of Alamar Blue (AbD Serotec) was added to each well, and the well plate was incubated for 3 h at 37°C. Fluorescence was measured at 570/600 nm in a Viento multispectrophotometer reader (Dainippon Pharmaceutical). The relative absorbance of CL6 cells without any treatment is regarded as 100% (it is indicated as a percent control in Fig. 4c).

Flow cytometric analysis

To count the numbers of EGFP-positive cells using PEI max-nanoparticles (0.8 μg/well in a six-well plate) on a magnetic sheet for 4 h (PEI max alone as a positive control), a Cytomics FC500 (Beckman Coulter Inc.) was used, and data were analyzed with FlowJo Ver.7 (Tree Star Inc.). Each sample was compared with negative control cells (without treatment).

Statistical analysis

Results, shown as the mean ± standard error (SE), were compared by analysis of variance (ANOVA) followed by Scheffe test (http://chiryo.phar.nagoya-cu.ac.jp/javastat/JavaStat-j.htm), with $P < 0.05$ considered significant.

Results

Characterization of PEI max-nanoparticles

Magnetic nanoparticles were well coated with PEI max and were highly dispersed in PEI max solution (1 mg/ml) or deionized water. Secondary size of the PEI max-nanoparticles was approximately 121.32 ± 27.36 nm (Fig. 2A). To evaluate stability in PEI max solution (1 mg/ml) or deionized water, we measured the ζ-potential of PEI max-nanoparticles, which was +45.53 mV in PEI max solution and +30.05 mV in deionized water. The PEI max-nanoparticles were aggregated by magnetic force (Fig. 2Ba) and quickly redispersed by vortex (Fig. 2Bb). Time-lapse photography (30 s/s) shows that magnetic nanoparticles were gradually removed at the site of the neodymium magnet (right side of the tube) for 2 h (magnetic nanoparticles for transfection: http://www.youtube.com/watch?v=Hyjfc4moHK4). These nanoparticles in PEI max solution were not aggregated without magnetic force. To avoid aggregation of plasmid-attached PEI max-nanoparticle caused by charge neutralization, it was necessary that their weight ratio was approximately 1:400 (Fig. 2C). In general, 1–2 μg of plasmid per well was mixed with the transfection reagent such, as PEI max, and FuGENE HD into six-well plates. However, too much (400–800 μg of nanoparticle per well) caused inhibition of transfection (described later). To solve the problem, we decided to use in 1 mg/ml of PEI max solution as a solvent. As a result, each concentration of the plasmid did not aggregate with PEI max-nanoparticle (Fig. 2Bb). To evaluate whether the plasmid DNA was attached to PEI max-nanoparticles in deionized water, we reacted PEI max-nanoparticles with plasmid DNA for 15 min at room temperature. Measuring the concentration of plasmid DNA in the upper layer (hyaline layer), the weight of PEI max-nanoparticles was reduced in a dependent manner (Fig. 2D).

Transfection efficiency using PEI max-nanoparticles and magnetic sheet, and viability of the CL6 cells treated with PEI max-nanoparticles

CL6 cells were transfected with pCAGGS-EGFP and PEI max alone as a positive control (Fig. 3a) and pCAGGS-EGFP and PEI max-nanoparticles (Fig. 3b) at 48 h after transfection. Many EGFP-positive cells were observed among CL6 cells transfected with PEI max-nanoparticles compared with those transfected with PEI max. To evaluate the optimum condition of transfection using PEI max-nanoparticles, quantitative real-time RT-PCR was performed at 48 h after transfection. The optimum condition of transfection was a concentration of 0.8 μg/well (Fig. 4a) on a magnetic sheet for 4 h (Fig. 4b). *EGFP* gene expression level was reduced under transfection of excess magnetic nanoparticles (7.5 μg/well) (Fig. 4a) and prolonged time on the magnetic sheet (24 h) (Fig. 4b). EGFP expression in CL6 cells transfected with PEI max-nanoparticles was increased approximately two to fourfold compared with those transfected with PEI max. The viability of CL6 cells treated with PEI max-nanoparticles, as measured by Alamar Blue assay, did not differ between cells treated with/without PEI max alone (Fig. 4c).

Number of EGFP-positive cells by flow cytometric analysis

Forty-eight hours after transfection using PEI max alone or PEI max-nanoparticles, we examined the number of EGFP-positive cells (total 10,000 cells) by flow cytometric analysis. Compared with the negative control (untreated CL6 cells), 42.2 ± 8.5% of cells treated with PEI max alone (Fig. 5a), 81.1 ± 4.0% of cells treated with 0.8 μg of PEI max-nanoparticles per well on the magnetic sheet for 4 h (Fig. 5b), and 13.9 ± 1.1% of cells treated with FuGENE HD (Fig. 5c) expressed EGFP. The number of EGFP-positive cells was significantly increased (approximately twofold) using PEI max-nanoparticles.

Discussion

In this study, to express target gene with high efficiency and low cytotoxicity, we focused on PEI max and magnetic nanoparticles (γ-Fe_2O_3). Many researchers have reported various transfection methods using PEI and magnetic nanoparticles, such as γ-Fe_2O_3, and superparamagnetic iron oxide nanoparticle (used as magnetic resonance imaging contrast agents) (Table 1). However, these methods had a low transfection efficiency [14, 15], combined with virus (adenovirus, or retrovirus) [15], and high cytotoxicity (low cell viability) [13] and may therefore have little effectiveness for clinical use.

The expression level of the *EGFP* gene was reduced under transfection of excess magnetic nanoparticles (7.5 μg/well) (Fig. 4a). This result may indicate that a high concentration of PEI max-nanoparticles formed the large agglutinate complexes with plasmid DNAs [22, 23]